

# Fatigue-Crack Propagation Behavior of Ductile/Brittle Laminated Composites

D.R. BLOYER, K.T. VENKATESWARA RAO, and R.O. RITCHIE

A study has been made of the fatigue-crack propagation properties of a series of laminated Nb-reinforced Nb<sub>3</sub>Al intermetallic-matrix composites with varying microstructural scale but nominally identical reinforcement volume fraction (20 pct Nb). It was found that resistance to fatigue-crack growth improved with increasing metallic layer thickness (in the range 50 to 250  $\mu\text{m}$ ) both in the crack-divider and crack-arrester orientations. For a given layer thickness, however, the properties in the crack-arrester orientation were superior to the crack-divider orientation. Indeed, the fatigue resistance of the crack arrester laminates was better than the fatigue properties of unreinforced Nb<sub>3</sub>Al and pure Nb; both laminate orientations had significantly better fatigue properties than Nb-particulate reinforced Nb<sub>3</sub>Al composites. Such enhanced fatigue performance was found to result from *extrinsic* toughening in the form of bridging metal ligaments in the crack wake, which shielded the crack tip from the applied (far-field) driving force. Unlike particulate-reinforced composites, such bridging was quite resilient under cyclic loading conditions. The superior crack-growth resistance of the crack-arrester laminates was found to result from additional *intrinsic* toughening, specifically involving trapping of the entire crack front by the Nb layer, which necessitated crack renucleation across the layer.

## I. INTRODUCTION

THE fracture properties of ductile-phase reinforced laminated brittle-matrix composites have been studied in some detail over the past decade with the objective of improving their crack-growth resistance for aerospace structural applications requiring reduced weight and increased mechanical performance. Such research has generally focused on the constrained deformation behavior of the ductile second phase and the matrix-reinforcement interfacial properties,<sup>[1-6]</sup> although effects of reinforcement volume fraction,<sup>[7]</sup> laminate orientation,<sup>[7,8,9]</sup> and microstructural scale of the layers<sup>[7,10-14]</sup> have all been examined. For example, laminates based on the Nb/Nb<sub>3</sub>Al and Nb/ or TiNb/ $\gamma$ -TiAl systems have been reported to show toughnesses exceeding 10 MPa $\sqrt{\text{m}}$  (e.g., compared to  $K_{Ic}$  values of 1 MPa $\sqrt{\text{m}}$  for Nb<sub>3</sub>Al<sup>[10]</sup>), which result from the significant plastic energy dissipation in large bridging zones that are typically observed behind the crack tip.

Despite efforts to improve the toughness of brittle-matrix laminates, little attention has been paid to their performance under cyclic loading. This can be critical for intermetallic-matrix composites because cyclic fatigue loading often promotes subcritical crack growth in the reinforcements themselves, thereby diminishing the bridging zone in the crack wake and correspondingly reducing the fatigue crack-growth resistance of the composite.<sup>[8]</sup> Such behavior has been observed in ductile metal reinforced brittle-matrix

composites using particulate, fiber, and disc-shaped reinforcements.<sup>[7,8,15,16]</sup> Specifically, for "laminar-like" composites of TiNb disc reinforced  $\gamma$ -TiAl composites, it was found that the orientation of the composite had strong influence on fatigue performance.<sup>[7,8]</sup> When the discs were aligned in the crack-divider or edge orientation, the fatigue properties of the composite were inferior to the unreinforced matrix, whereas with the discs aligned in the crack-arrester or face orientation, the composite displayed marginally better fatigue resistance (Figure 1). However, apart from this study, reports of the effect of microstructure and composite orientation on fatigue crack-growth resistance in ductile-metal reinforced brittle-matrix laminates have not been available.

Accordingly, the current work addresses the influence of reinforcement morphology, orientation, and metal layer thickness on the fatigue crack-growth resistance of laminated Nb-reinforced Nb<sub>3</sub>Al intermetallic composites. The study focuses on three laminate layer thicknesses (at a nominally constant volume fraction of 20 pct) in both the divider and arrester orientations. Results are compared with previous examinations of *in situ* particulate-reinforced Nb/Nb<sub>3</sub>Al composites to show the effectiveness of coarser-scale, high aspect-ratio reinforcements in promoting crack-growth resistance.

## II. EXPERIMENTAL PROCEDURES

### A. Laminate Processing

Two laminate orientations, the crack arrester and crack divider (Figure 1), were prepared in three different layer thickness combinations: (1) 50  $\mu\text{m}$  Nb/200  $\mu\text{m}$  Nb<sub>3</sub>Al, (2) 125  $\mu\text{m}$  Nb/500  $\mu\text{m}$  Nb<sub>3</sub>Al, and (3) 250  $\mu\text{m}$  Nb/1000  $\mu\text{m}$  Nb<sub>3</sub>Al.

This gave a nominally constant reinforcement volume fraction in each laminate of  $f \sim 0.2$ .

---

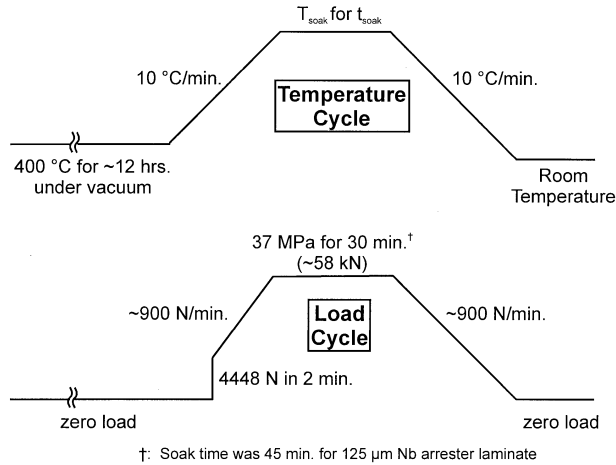
D.R. BLOYER, Postdoctoral Researcher, and R.O. RITCHIE, Professor, are with the Materials Sciences Division, Lawrence Berkeley National Laboratory, and Department of Materials Science and Mineral Engineering, University of California, Berkeley, CA 94720-1760. K.T. VENKATESWARA RAO, formerly Research Engineer with the Department of Materials Science and Mineral Engineering, University of California, is Manager, R&D, Vascular Intervention Group, Guidant Corporation, Santa Clara, CA 95052.

Manuscript submitted June 5, 1998.

## Arrester Orientation    Divider Orientation



Fig. 1—Schematic illustrations of the arrester and divider orientations in the laminates.



Laminate	Soak Temperature $T_{\text{soak}}$	Soak Time $t_{\text{soak}}$
50 $\mu\text{m}$ Nb/200 $\mu\text{m}$ Nb <sub>3</sub> Al (arrester and divider)	1500 °C	25 min.
125 $\mu\text{m}$ Nb/500 $\mu\text{m}$ Nb <sub>3</sub> Al (divider)	1650 °C	25 min.
250 $\mu\text{m}$ Nb/1000 $\mu\text{m}$ Nb <sub>3</sub> Al (arrester and divider)		
125 $\mu\text{m}$ Nb/500 $\mu\text{m}$ Nb <sub>3</sub> Al (arrester)	1680 °C	40 min.

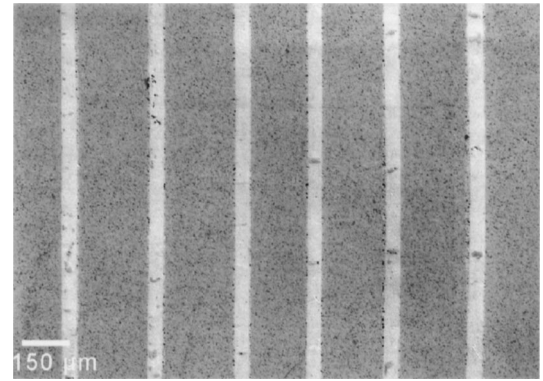
Fig. 2—Temperature and pressure profiles used in the processing of the Nb/Nb<sub>3</sub>Al laminated composites.

Nb<sub>3</sub>Al powder was prepared by reaction synthesis of elemental Nb (CERAC Inc., Milwaukee, WI; 99.8 pct, -325 mesh for 125 and 250  $\mu\text{m}$  Nb laminates, and CERAC Inc., 99.8 pct, 5  $\mu\text{m}$  or less for the 50  $\mu\text{m}$  Nb laminates) and Al (Valimet Co., Stockton, CA; 99.3 pct, -325 mesh) powders in the molar ratio 0.76Nb:0.24Al. These were mixed in a ball mill for ~0.5 hours and then heated in a helium atmosphere at 1400 °C for 4 hours to form Nb<sub>3</sub>Al. The reacted powder was subsequently ball milled for ~0.5 hours and reheated to 1400 °C for an additional 4 hours to complete the reaction. The Nb<sub>3</sub>Al powder was ball milled again for 1 hour to reduce any agglomerated particles prior to use in composite fabrication.

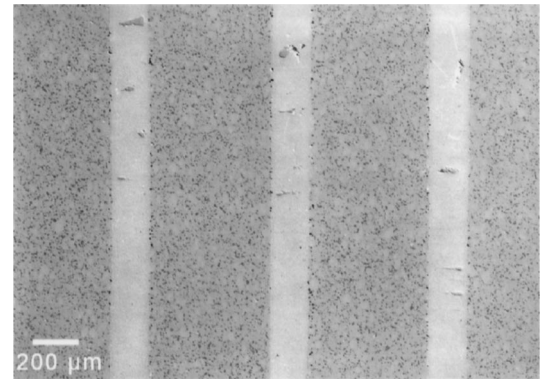
The laminates were prepared by sequentially cold pressing layers of the Nb<sub>3</sub>Al powder between the Nb foils (Rembar Co., Dobbs Ferry, NY, and ALFA/AESAR\*, 99.8 pct)

\*ALFA/AESAR is a trademark of Johnson Matthey Co., Ward Hill, MA.

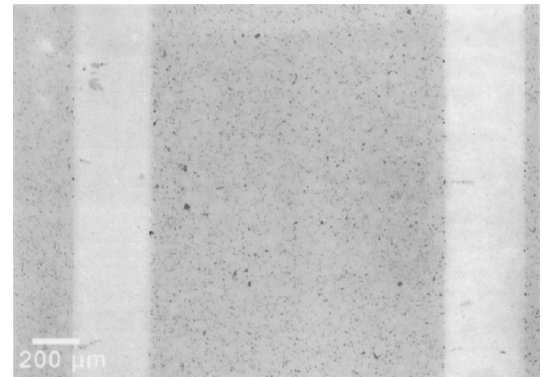
in a graphite mold and then hot pressing in an argon atmosphere to create composite cylinders or discs. The laminates were hot pressed according to the temperature and



(a)



(b)



(c)

Fig. 3—Scanning electron micrographs of the composite microstructure for the (a) 50  $\mu\text{m}$  thick Nb/200  $\mu\text{m}$  thick Nb<sub>3</sub>Al, (b) 125  $\mu\text{m}$  thick Nb/500  $\mu\text{m}$  thick Nb<sub>3</sub>Al, and (c) 250  $\mu\text{m}$  thick Nb/1000  $\mu\text{m}$  thick Nb<sub>3</sub>Al laminates. (The apparent extraneous grains in the Nb phase are actually artifacts of the polishing, which accentuates specific grains.)

pressure profiles given in Figure 2. The resultant microstructures consisted of evenly spaced, parallel layers of Nb<sub>3</sub>Al intermetallic separated by layers of Nb metal (Figure 3).

The grain sizes of the Nb and Nb<sub>3</sub>Al layers were determined in polished and etched composite specimens using a simple line intercept method (etchant: standard Nb etch no. 164 in 1992 ASTM Standard E407). This gave average Nb<sub>3</sub>Al grain sizes of  $4 \pm 2$  and  $10 \pm 6$   $\mu\text{m}$  for the laminates processed at 1500 °C and 1650 °C to 1680 °C, respectively. Similarly, average grain sizes of  $99 \pm 31$ ,  $222 \pm 112$ , and  $300 \pm 123$   $\mu\text{m}$  were observed for the 50, 125,

**Table I. Effective Reinforcement Thickness and Volume Fractions**

Target Nb Thickness ( $\mu\text{m}$ )	Effective Nb Thickness ( $\mu\text{m}$ )	Effective Nb Volume Fraction* ( $f$ )
<u>Arrester orientation</u>		
50	40	0.16
125	85	0.14
250	218	0.17
<u>Divider orientation</u>		
50	40	0.16
125	95	0.15
250	218	0.17

\*Target volume fraction  $f = 0.2$ .

and 250  $\mu\text{m}$  Nb layers, respectively. During processing, however, the Nb grains grew in such a manner that they encompassed the entire thickness of the metal layer. As a result, the grain sizes were measured as a “linear” grain size along the length of the metal layer with the grain thickness being that of the Nb reinforcing layer.

X-ray line scans indicated there was some diffusion of aluminum into the Nb reinforcing layers, thus creating a reaction layer between the metal and intermetallic. This reaction layer was treated as an effective reduction in the thickness of the Nb reinforcing layer and an effective increase in the thickness of the  $\text{Nb}_3\text{Al}$  matrix layer. The resulting small differences in the effective reinforcement volume fractions and layer thicknesses are listed in Table I.

### B. Mechanical Testing and Specimen Preparation

The divider laminates were prepared as disc-shaped compact-tension DC(T) specimens with thicknesses of  $B \sim 3$  to 5 mm and widths of  $W \sim 33$  mm. Corresponding arrester laminates were tested either as single-edge-notched four-point bend SE(B) beams (inner and outer spans of  $\sim 10$  and 35.5 mm, respectively) for 50  $\mu\text{m}$  thick Nb ( $B \sim 3.5$  mm,  $W \sim 9.5$  mm) and 250  $\mu\text{m}$  thick Nb ( $B \sim 3.5$  mm,  $W \sim 13.5$  mm) laminates or compact-tension C(T) specimens ( $B \sim 3.5$  mm,  $W \sim 25.4$  mm) for the 125  $\mu\text{m}$  thick Nb laminate.

Samples were cycled on automated electrohydraulic testing machines operating under stress-intensity,  $K$ , control in controlled room air (22 °C, 45 pct relative humidity) at load ratios (ratio of minimum to maximum applied loads) of  $R = 0.1$  and 0.5 with a test frequency of 25 Hz (sine wave). The divider samples were cycled under decreasing stress-intensity range conditions with a normalized  $K$  gradient (load shedding rate) of 0.1  $\text{mm}^{-1}$ ; corresponding testing for the arrester samples was performed under constant stress-intensity range conditions. Alternating and maximum threshold stress-intensity levels,  $\Delta K_{TH}$ ,  $K_{max,TH}$ , were operationally defined at a growth rate of  $10^{-10}$  m/cycle.

In both orientations, crack length was monitored by unloading compliance measurements using a back-face strain gage (resolution  $\sim 100$   $\mu\text{m}$  of crack extension), with readings verified *in situ* by direct optical measurements using a Questar short focal-length telescope. Because the effect of bridging decays under cyclic loading, the differences be-

tween the compliance and optical measurements were within 10 pct.\* For the arrester specimens, plots of crack

\*In this article, we consider the crack configuration as one of a crack at furthest extent with a bridging zone behind the crack tip, rather than a shorter crack with microcracking ahead of the tip in a process zone.

length,  $a$ , vs number of cycles,  $N$ , over roughly three Nb/ $\text{Nb}_3\text{Al}$  layers of crack extension were made, with average crack-growth rates computed from the slopes of best-fit lines through the  $a$  vs  $N$  data at each stress-intensity level. Linear elastic stress intensity  $K$  values were calculated from standard handbook solutions. Data are presented in the form of the crack-growth rates,  $da/dN$ , as a function of either the applied (far-field) alternating ( $\Delta K$ ) or maximum ( $K_{max}$ ) stress intensities.

## III. RESULTS AND DISCUSSION

### A. Fatigue Crack-Growth Behavior

Fatigue-crack growth rates for the three Nb/ $\text{Nb}_3\text{Al}$  laminate systems in the divider and arrester orientations are plotted in Figures 4 and 5, respectively. Corresponding fracture toughness/resistance curve (R-curve) data for these materials, taken from Reference 14, are summarized in Table II. Compared to behavior under monotonic loading,<sup>[14]</sup> resistance to crack growth is diminished under cyclic loads. Specifically, fatigue-crack growth occurs at stress intensities just below that necessary for crack initiation on the resistance curve, and the maximum stress-intensity levels that can be supported by the laminates are reduced to some 50 pct of the maximum fracture toughness values. As discussed subsequently, the mechanism for such diminished crack-growth resistance under cyclic, compared to monolithic, loading can be related to a degradation of crack-tip shielding, specifically from crack bridging by intact Nb layers. It is important to note, however, that the resistance to crack growth in both orientations is enhanced with increasing Nb layer thickness, and, in common with most materials, the fatigue-crack growth rates (at a fixed  $\Delta K$ ) are increased with increasing (positive) load ratios.

Despite the detrimental effects of cyclic loading, Figures 4 and 5 show that the addition of Nb as a laminated phase significantly improves the fatigue crack-growth resistance of the  $\text{Nb}_3\text{Al}$  intermetallic. Unreinforced  $\text{Nb}_3\text{Al}$  essentially shows no fatigue behavior and is thus represented as a near vertical line at the stress intensity where cracking becomes catastrophic, *i.e.*, at  $K_{Ic} \sim 1$   $\text{MPa}\sqrt{\text{m}}$ . In comparison, threshold  $\Delta K_{TH}$  levels in the laminate were a factor of  $\sim 4$  to 6 times ( $\sim 3$  to 7  $\text{MPa}\sqrt{\text{m}}$ ) higher, depending on the composite layer thickness and orientation. Moreover, these threshold  $\Delta K_{TH}$  levels are  $\sim 130$  to 230 pct higher than reported<sup>[16,17]</sup> for Nb/ $\text{Nb}_3\text{Al}$  *in situ* composites, where the Nb reinforcement was in the form of a particulate (at twice the volume fraction of the current laminates). Based upon these comparisons, laminate reinforcements appear to be an excellent choice for improving the fatigue crack-growth properties of brittle intermetallics through the incorporation of a ductile second phase. The properties, however, are a strong function of orientation, as discussed subsequently.

#### 1. Crack-divider orientation

Figure 4(a) shows that there is also a significant improvement in the fatigue crack-growth resistance of the divider

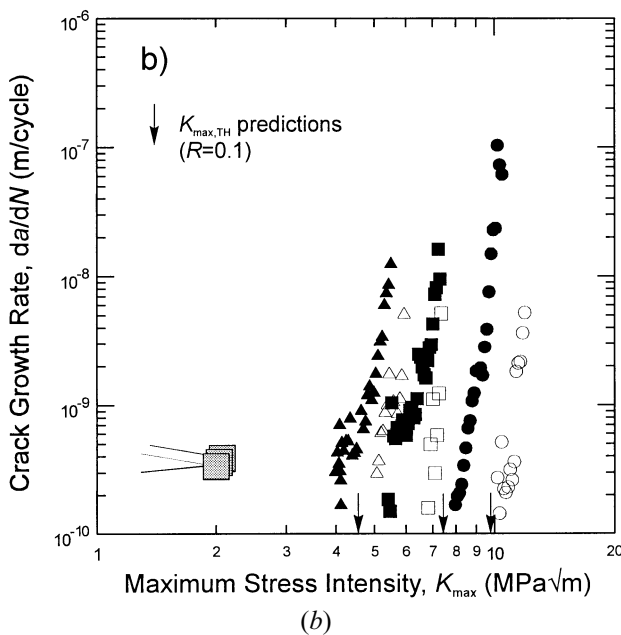
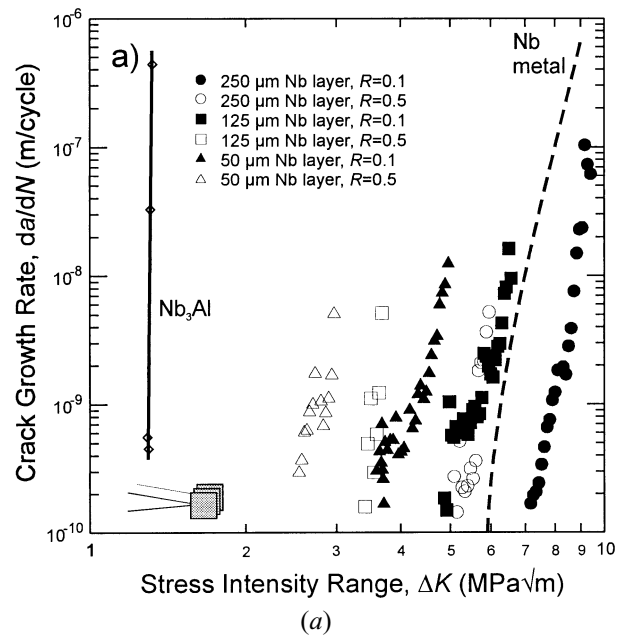


Fig. 4—Variation in fatigue-crack propagation rates,  $da/dN$ , at  $R = 0.1$  and  $0.5$  in the crack-divider Nb/Nb<sub>3</sub>Al laminates as a function of (a) the applied stress-intensity range,  $\Delta K$ , and (b) the maximum stress intensity,  $K_{max}$ , showing the improved crack-growth resistance with increasing reinforcement layer thickness. Note how the load ratio data are not normalized by either  $\Delta K$  or  $K_{max}$ , in common with many intermetallics. The model predictions for the fatigue thresholds,  $K_{max,TH}$ , in the Nb/Nb<sub>3</sub>Al crack-divider laminate (marked by vertical arrows for the 50, 125, and 250  $\mu\text{m}$  Nb laminates, respectively) are calculated using the weight-function method described by Eq. [6]. The labeling of the data points, specified in (a), is the same for both plots.

laminates with increasing reinforcement layer thickness, yet the properties of the composite are essentially bound by the fatigue crack-growth resistance of unreinforced Nb<sub>3</sub>Al and Nb metal (Figure 4(a)). Threshold  $\Delta K_{TH}$  values at  $R = 0.1$  increase from  $\sim 3.5$  to  $5$  to  $7$  MPa $\sqrt{\text{m}}$  for the 50, 125, and 250  $\mu\text{m}$  thick Nb laminates, respectively. At  $R = 0.5$ ,  $\Delta K_{TH}$  values similarly are increased with increasing layer thickness, but are  $\sim 30$  pct lower than at  $R = 0.1$ .

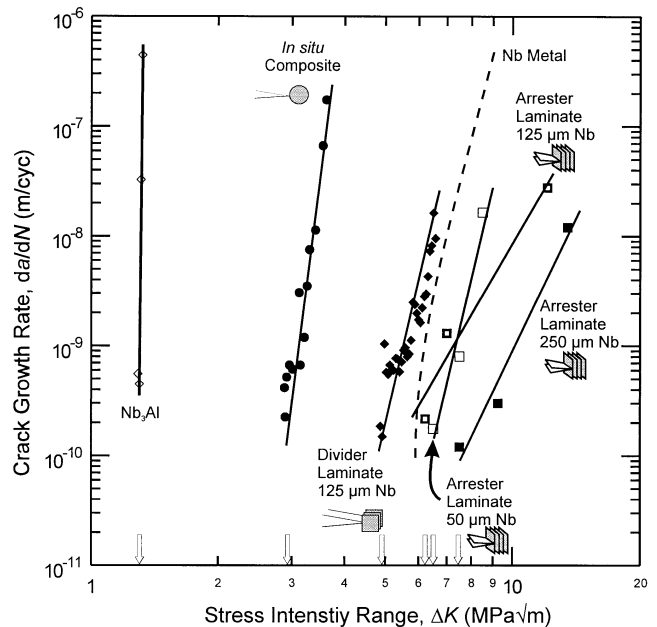


Fig. 5—Variation in fatigue-crack propagation rates,  $da/dN$ , at  $R = 0.1$  in the crack-arrester Nb/Nb<sub>3</sub>Al laminates as a function of the applied stress-intensity range,  $\Delta K$ , again showing improved crack-growth resistance with increasing reinforcement layer thickness. Crack-growth properties for the three laminate structures are shown to be superior to that of unreinforced Nb<sub>3</sub>Al, a Nb-particulate reinforced (*in situ*) Nb<sub>3</sub>Al composite, and even metallic Nb. Results for the 125  $\mu\text{m}$  thick Nb crack-divider laminate (from Fig. 4(a)) are shown for comparison. Vertical arrows represent the threshold  $\Delta K_{TH}$  values.

Table II. Summary of Toughness/R-Curve Results<sup>14</sup>

Nominal Nb Thickness ( $\mu\text{m}$ )	$K_0^*$ (MPa $\sqrt{\text{m}}$ )	Predicted $K_{ss}^{**}$ (MPa $\sqrt{\text{m}}$ )	Measured $K_{ss}^\dagger$ (MPa $\sqrt{\text{m}}$ )
<b>Arrester orientation</b>			
50	7.3	15.5	13 – 15
125	9	18.4	15 – 20
250	10.4	$\sim 33^\ddagger$	10 – 20
<b>Divider orientation</b>			
50	$\sim 1^\S$	$\sim 13^\ddagger$	11
125	$\sim 1^\S$	$\sim 20^\ddagger$	15
250	$\sim 1^\S$	$\sim 27^\ddagger$	20

\*Crack-initiation toughness.

\*\*Predicted from Eqs. [3] and [4] (Section III-B).

†Estimated from the peak toughness on the R-curve.

§Approximate values, as measured values were higher due to residual bridging left after precracking.<sup>14</sup>

‡Predicted using an energy-based method as described in Ref. [14].

Crack tunneling in the brittle intermetallic layers during the decreasing  $\Delta K$  tests (Figure 6) appeared to be responsible for the formation of bridging zones of uncracked Nb layers in the divider orientation. This is in contrast to ductile-particle toughened intermetallics, such as in TiNb-reinforced  $\gamma$ -TiAl, where such bridging zones, which form readily under monotonic loading, are essentially eliminated under cyclic loading due to fatigue failure of the ductile ligaments.<sup>[8]</sup> Metallographic sections of DC(T) specimens taken after testing revealed bridging zone sizes of  $\sim 1$ , 3, and 5 mm for the 50, 125, and 250  $\mu\text{m}$  Nb laminates, respectively; this is to be compared with bridging zones of

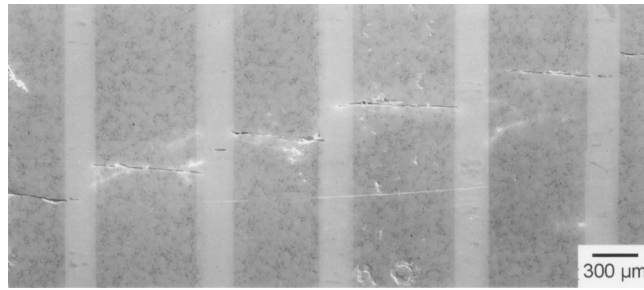
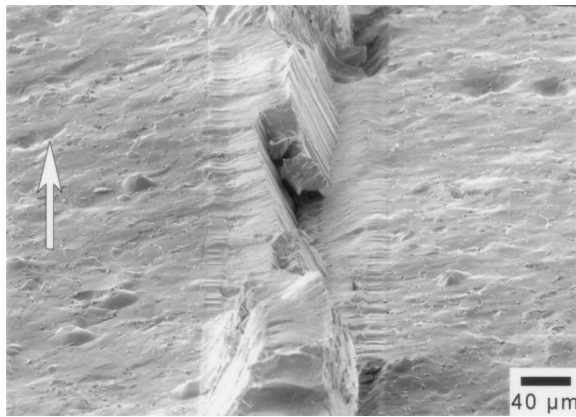
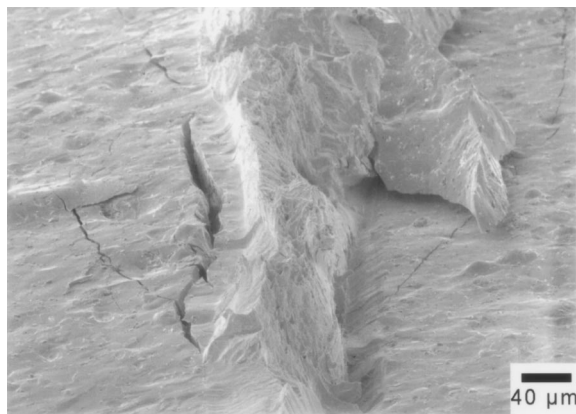


Fig. 6—Scanning electron micrograph showing a cross section of a Nb/Nb<sub>3</sub>Al crack-divider laminate showing crack tunneling, by non-coplanar cracking, in the intermetallic layers during fatigue-crack growth. The crack-growth direction is into the page.



(a)



(b)

Fig. 7—Scanning electron micrographs (taken at a ~80 deg tilt angle) of (a) fatigue fracture surface of the Nb reinforcing layer and (b) corresponding failure of the Nb layer under monotonic loading (during R-curve testing) in the Nb/Nb<sub>3</sub>Al crack-arrester laminates. Note in (a) the absence of interfacial cracking and extensive plastic deformation in the fatigue failure but the presence of parallel markings. The vertical arrow represents the general direction of crack growth.

**Table III. Modified Paris Equation Exponents for Divider Laminates**

Nb/Nb <sub>3</sub> Al Layer Thickness	50 μm Nb/200 μm Nb <sub>3</sub> Al	125 μm Nb/500 μm Nb <sub>3</sub> Al	250 μm Nb/1000 μm Nb <sub>3</sub> Al
<i>p</i>	3	3	10
<i>n</i>	7	8	13

4 to 9 mm observed under monotonic loads during R-curve testing.<sup>[14]</sup> Although there is clearly some degradation in the bridging under cyclic loading, these zones can still provide sizable crack-tip shielding under fatigue loading conditions. The improved fatigue crack-growth resistance for the thicker layered composite can be attributed to the larger crack-tip shielding zones associated with the increased thickness of the Nb layers.

The fracture surfaces of the Nb reinforcing layers (Figure 7(a)) did not show evidence of gross plastic deformation and failure by microvoid coalescence, as noted during monotonic loading conditions (Figure 7(b)). Instead, the smaller bridging zones under cyclic loading appeared to result from the failure of Nb layers by fatigue cracking, as evidenced by the parallel markings on the Nb fracture surfaces (Figure 7(a)). No changes in fracture surface morphology were found at different  $\Delta K$  levels.

The resiliency of the bridging zones under cyclic loading and the consequent crack-growth resistance of the divider laminates are due in part to the manner in which the crack tunnels in the Nb<sub>3</sub>Al intermetallic layers. Cross sections behind the crack tip in the divider laminates indicated that non-coplanar cracks formed in the intermetallic on either side of the Nb layer (Figure 6); the highly angled fatigue fracture surfaces of the Nb reinforcing layers (Figure 7(a)) were consistent with this offset cracking. Such crack path offset and tortuosity have been shown in monotonic crack-growth studies to promote toughening of laminates by increasing the energy required to fail the bridging layer.<sup>[3,6]</sup>

With respect to the crack-growth rates under cyclic loading, by fitting the low *R* data to a simple Paris power-law expression,<sup>[18]</sup>

$$\frac{da}{dN} = C \Delta K^m \quad [1]$$

where *C* and *m* are scaling constants, the exponents for the divider orientation were found to be *m* ~ 10, 11, and 23 for the 50, 125, and 250 μm thick Nb laminates, respectively. These exponents are considerably higher than commonly seen with ductile metallic materials, yet they are consistent with measured values for most intermetallics, which range typically between 10 and 20.

Equation [1], however, relates growth rates solely to  $\Delta K$ , whereas in brittle solids, it is important to additionally account for the role of  $K_{\max}$  in affecting growth-rate behavior. This is critical, as replotting the growth-rate data in terms of  $K_{\max}$  (Figure 4(b)) narrows the spread of the data, yet, unlike behavior in ceramics, does not fully normalize it with respect to variations in load ratio. The separate dependencies of  $\Delta K$  and  $K_{\max}$ , however, can be represented by expressing the *R* = 0.1 and 0.5 data in terms of a modified Paris equation:<sup>[19]</sup>

$$\frac{da}{dN} = C' \Delta K^p K_{\max}^n \quad [2]$$

where *C'* is a constant equal to  $C(1 - R)^n$  and  $n + p = m$ . Exponents for each layer thickness are shown in Table III, where it can be seen that  $K_{\max}$ , more so than  $\Delta K$ , has a significant influence on the crack-growth process in Nb/Nb<sub>3</sub>Al.

These results are similar to those reported for several other intermetallic systems in that (1) neither  $\Delta K$  nor  $K_{\max}$

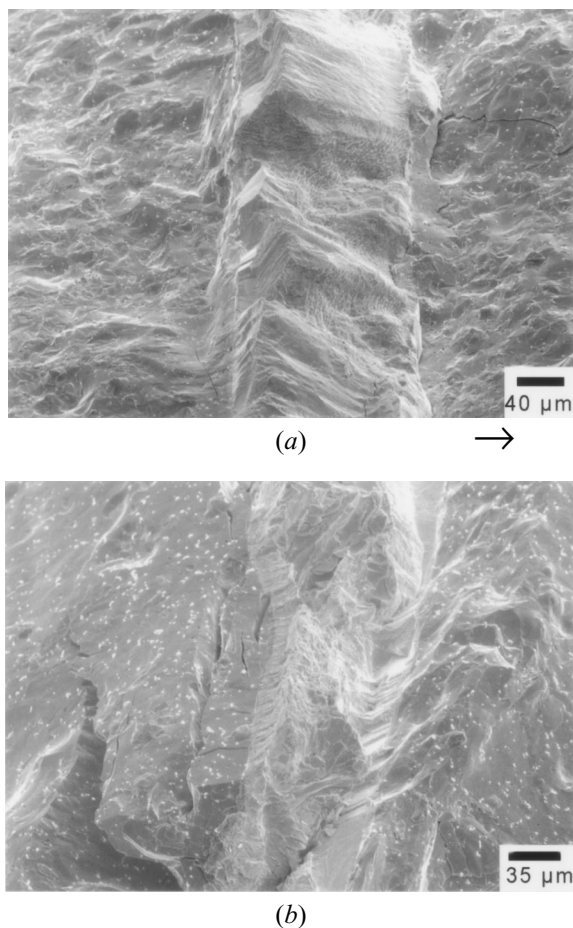


Fig. 8—Scanning electron micrographs (taken at a  $\sim 60$  deg tilt angle) of (a) fatigue fracture surface of the Nb reinforcing layer (at  $\Delta K \sim 12$  MPa $\sqrt{m}$ ) and (b) corresponding failure of the Nb layer under monotonic loading (during R-curve testing) in the Nb/Nb<sub>3</sub>Al crack-divider laminates. Note as in Fig. 7 the absence of interfacial cracking and extensive plastic deformation in the fatigue failure in (a) but, again, the presence of parallel markings. Horizontal arrows represent the general direction of crack growth.

alone can fully account for the role of load ratio, and (2) the dependency of growth rates on  $K_{max}$  is comparable, yet larger, than the  $\Delta K$  dependence, *i.e.*,  $n > p$  (*e.g.*, Reference 20). In ductile materials (*e.g.*, metals), where  $n < p$ , the  $\Delta K$  dependence is ascribed to the cyclic damage process ahead of the crack tip (*e.g.*, alternating crack-tip blunting and resharpening), whereas the smaller  $K_{max}$  dependence primarily results from crack closure at lower  $\Delta K$  levels and  $K_{max}$ -controlled fracture mechanisms (“static modes”) at high, near instability levels (*e.g.*, References 21 and 22). In brittle materials (*e.g.*, ceramics), conversely, where  $n \gg p$ , the dominant  $K_{max}$  dependence results from  $K_{max}$ -controlled crack-advance mechanism(s) (*e.g.*, intergranular cracking), whereas the smaller  $\Delta K$  dependence is associated with a cyclic loading induced decay in the crack-tip shielding (*i.e.*, R-curve toughening) mechanism(s) behind the crack tip.<sup>[23,24]</sup>

The fractographic and metallographic evidence discussed previously indicates that the present behavior in the intermetallic laminates is related to a similar series of mechanistic processes, specifically (1) the cracking of the Nb<sub>3</sub>Al intermetallic matrix, which is clearly  $K_{max}$  controlled;<sup>[16,17]</sup> (2) fatigue cracking in the Nb layers, which is primarily

$\Delta K$  controlled; and finally (3) the progressive degradation of a bridging zone of intact Nb layers behind the crack tip, due to fatigue cracking in these layers, which is also  $\Delta K$  controlled.

## 2. Crack-arrester orientation

The arrester laminates showed similar trends in fatigue-crack growth behavior, although their crack-growth properties were superior to the divider laminates at each layer thickness (Figure 5). Thresholds and crack-growth curves, however, were far less affected by the Nb layer thickness; indeed,  $\Delta K_{TH}$  values were all between 6 to 7.5 MPa $\sqrt{m}$  and similar to that measured for unreinforced Nb metal (prepared under equivalent processing conditions). As with the divider orientation, the fatigue crack-growth resistance was generally improved with increased Nb layer thickness.

The crack/layer interactions in the arrester laminates showed many similarities to those of the divider laminates with the fatigue fracture surface (Figure 8(a)), showing a general lack of void coalescence and near interfacial cracking as seen in the monotonic fracture surface (Figure 8(b)). Fracture surfaces were similar and striation-like markings were again observed in the regions where the Nb layers had failed by fatigue (*e.g.*, Figure 8(a)). Akin to the divider laminates, such fatigue cracking acted to reduce bridging zone sizes by more than 50 pct compared to those developed under monotonic loading.<sup>[14]</sup>

There were, however, specific differences in the mechanisms by which the crack propagated through the arrester, compared to the divider, laminates. The entire crack front can become trapped in the Nb reinforcing layer in the arrester orientation, whereas it is exposed to the intermetallic layer at all times for the divider orientation. This trapping of the crack in the arrester laminates leads to an additional mechanism of toughening in this orientation, *i.e.*, that of crack renucleation across the Nb layers. As this is an *intrinsic* toughening mechanism, it should not degrade under cyclic loading; however, as discussed subsequently, fatigue cracking through the layer at lower growth rates acts to minimize its effect.

Specifically, at low applied  $\Delta K$  levels, where the applied  $K_{max}$  was below the initiation fracture toughness,  $K_0$ , on the R-curve (*i.e.*, at a stress intensity lower than is necessary to renucleate the crack in the Nb<sub>3</sub>Al on the far side of a Nb layer), the crack was observed to impinge on the Nb reinforcing layer and grow through the metal layer prior to renucleation in the Nb<sub>3</sub>Al intermetallic on the far side of the layer. As a result, bridging ligaments in the crack wake were essentially eliminated (Figure 9(a)). Close to  $\Delta K_{TH}$ , the crack spends most of the time fatiguing through the Nb layer, whereas on exiting, it propagates across the intermetallic region in one cycle. This is consistent with the fact that thresholds for the arrester laminates are (1) similar to that of metallic Nb (prepared under equivalent processing conditions) and (2) only marginally affected by the composite layer thickness (Figure 5). Thus, it appears that the higher thresholds observed in this laminate orientation are the result of the intrinsically higher fatigue crack-growth resistance of the Nb reinforcing layer.

Indeed, unlike many ceramics, where there is no intrinsic mechanism of fatigue-crack advance such that the fatigue threshold,  $K_{max,TH}$ , approaches the value of the initiation toughness,  $K_0$ , on the R-curve, in the present intermetallic

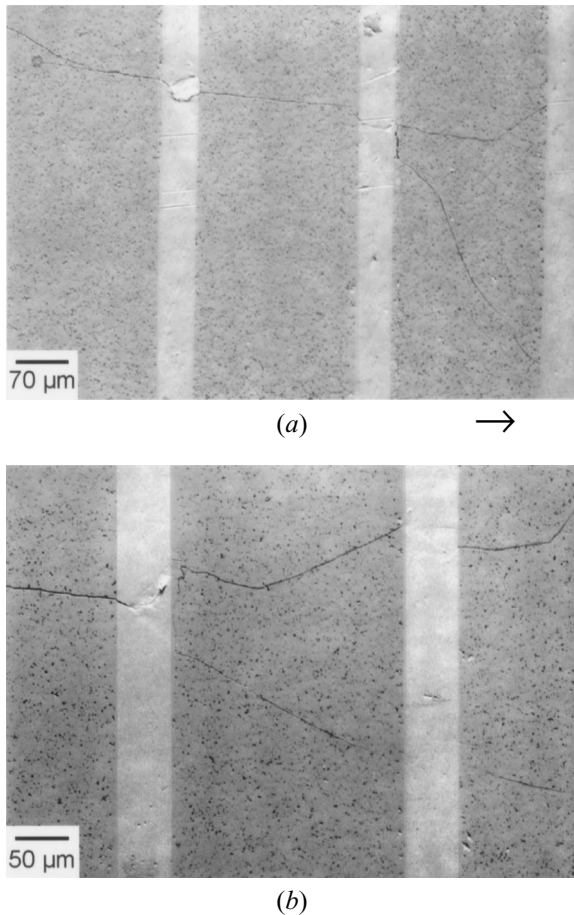


Fig. 9—Scanning electron micrographs of the crack profiles during fatigue-crack growth in the 50  $\mu\text{m}$  thick Nb crack-arrester laminate, illustrating behavior (a) at a constant  $\Delta K \sim 6.5 \text{ MPa}\sqrt{\text{m}}$  (where  $K_{\text{max}} < K_0$ , the initiation stress intensity on the R-curve), where the crack fatigues through all the Nb layers behind the crack tip, thereby limiting crack renucleation and crack bridging, and (b) at a constant  $\Delta K \sim 7.5 \text{ MPa}\sqrt{\text{m}}$  (where  $K_{\text{max}} > K_0$ ) showing that the crack has renucleated in the Nb<sub>3</sub>Al intermetallic across the Nb layer, leaving at least one (bridging) Nb layer intact behind the crack tip. The horizontal arrow represents the general direction of crack growth.

composites, where there is clearly an intrinsic fatigue mechanism in the Nb,  $K_{\text{max,TH}}$  is  $\sim 10$  to 20 pct lower than the values<sup>[14]</sup> of  $K_0$ .

In contrast, at the higher applied  $\Delta K$  levels (where  $K_{\text{max}} > K_0$ ), the crack renucleated in the Nb<sub>3</sub>Al, leaving the Nb layer intact, thus forming a small bridging zone in the crack wake (Figure 9(b)). Bridging zones extended about two Nb layers behind the crack tip, *i.e.*,  $\sim 0.5$  and  $2.5 \text{ mm}$ , respectively, for the 50 and 250  $\mu\text{m}$  thick Nb arrester laminates and about three Nb layers, *i.e.*,  $\sim 1.9 \text{ mm}$ , in the 125  $\mu\text{m}$  thick Nb laminate. These bridges act to shield the crack tip such that higher applied stress-intensity levels are required to drive the crack at growth rates above threshold.

Thus, based upon the observed interactions of the crack with the layered microstructures, the fatigue crack-growth resistance of the arrester laminates can be attributed to two primary contributions: (1) an intrinsic increase in fatigue threshold values due to the entire crack front being trapped in the Nb layer and (2) extrinsic shielding from crack bridging by intact Nb layers.

Finally, it should be noted in Figure 5 that the arrester

laminates display somewhat higher fatigue thresholds than metallic Nb. This is believed to result from the fact that the renucleation event across the Nb layers involved non-coplanar crack renucleation (Figures 9(a) and (b)), which caused angled fatigue fracture surfaces in the Nb layers (Figure 8(a)). An additional contribution may be due to constraint in the Nb reinforcing layer imposed by the surrounding intermetallic matrix.

### B. Crack-Growth Modeling

Under monotonic loading conditions, the shielding contribution due to crack bridging can be estimated using a weight function method to solve for the (local) stress intensity imposed at the crack tip.<sup>[25–30]</sup> Specifically, the closing forces imparted by the bridging ligaments are treated as a traction distribution that is integrated over the bridging zone length using a weighting function. The weighting function serves to appropriately weight the shielding from a traction at a specific point behind the crack tip and is dependent upon the geometry of the test specimen. Solutions for the specimen geometries used in the present work are given in the Appendix. The bridging contribution thus becomes

$$K_b = \int_L \sigma(x) h(a, x) dx \quad [3]$$

where  $\sigma(x)$  is the traction as a function of distance behind the crack tip,  $h(a, x)$  is the weight function, and the integration limits are determined by the bridging zone length,  $L$ . The shielding contribution can then be superposed with some intrinsic toughness of the composite,  $K_0$ , and the applied stress intensity,  $K_{\text{app}}$ , can be predicted as

$$K_{\text{app}} = K_0 + K_b \quad [4]$$

Using this approach, steady-state toughnesses on the R-curve have been predicted for this laminate system; results are shown in Table II and have been described in detail in Reference 14.

To model the corresponding fatigue crack-growth resistance of the laminates, the approach was modified by combining Eqs. [3] and [4] in terms of  $K_{\text{max}}$  and employing a traction function representative of the fatigue response of the reinforcing metal layers which form the bridging zones, *viz.*:

$$K_{\text{app,max}} = K_{0,\text{max}} + \int_{L_c} \sigma_f(x) h(a, x) dx \quad [5]$$

where  $K_{\text{app,max}}$  is the maximum stress intensity necessary to drive the crack, and  $K_{0,\text{max}}$  is the maximum intrinsic crack-growth resistance under fatigue loading. The second term on the right side of the equation is the maximum shielding stress intensity, where  $h(a, x)$  is the appropriate weight function,  $\sigma_f(x)$  is the fatigue-based traction that represents the bridging layers, and  $L_c$  is the bridging zone length under cyclic loading.

Since traction functions for ductile second-phase reinforcements under cyclic loading conditions have not been developed to date, as a first approximation, the traction functions developed from studies on crack growth in the Nb/Nb<sub>3</sub>Al laminates under monotonic loads<sup>[14]</sup> were used to

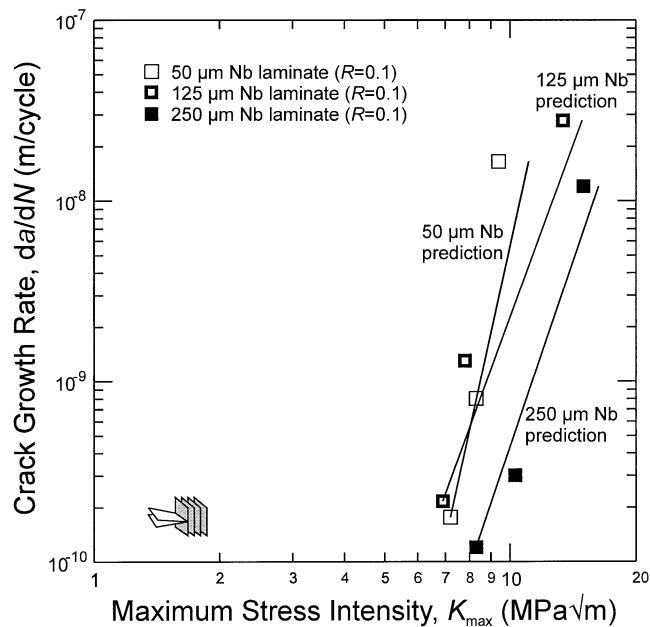


Fig. 10—Comparison of experimental data points and model predictions (lines) of fatigue-crack propagation rates in the Nb/Nb<sub>3</sub>Al crack-divider laminates with 50 μm thick Nb layers, 125 μm thick Nb layers, and 250 μm thick Nb layers. Predictions were calculated using the weight-function method described by Eq. [6].

estimate the expected fatigue response. Accordingly, Eq. [5] takes the form

$$K_{app,max} = K_{o,max} + f \sigma_c \int_{L_c} h(a, x) dx \quad [6]$$

where  $f$  is the effective volume fraction reinforcement (from Table I), and  $\sigma_c$  is the magnitude of the assumed constant traction function, which varies between 275 and 540 MPa, as listed in Reference 14. These equations were numerically integrated using a Romberg algorithm.

#### 1. Crack-divider orientation

As only the near-threshold bridging behavior is known for this orientation, calculations were focused on estimating the maximum stress intensity at the threshold,  $K_{max,TH}$ . Similar to the case of monotonic loading,<sup>[14]</sup>  $K_{o,max}$  for the divider laminates is equated to the intrinsic toughness of Nb<sub>3</sub>Al ~ 1 MPa√m. Thus, using the measured bridging zone lengths, the effective volume fractions (Table I), the traction functions,<sup>[14]</sup> and the weighting function for the DC(T) geometry (Eq. [A1] Table A1), threshold  $K_{max,TH}$  values were predicted for the 50, 125, and 250 μm thick Nb divider laminates. Predictions are shown in Figure 4(b) and indicate that the calculated thresholds are approximately 25 pct larger than the measured values. The overestimates presumably result from the limiting assumptions of the analysis. First, it is unlikely that the traction functions for monotonic and cyclic loading are identical. Although there is no precedence for the nature of the change in the traction function with cyclic loading, the extent of bridging in many ductile-phase reinforced composites is known to be diminished in fatigue; however, this effect appears to be minimized with the present laminated composites. Second, the assumption that the traction function is a constant is also somewhat questionable, although this approach has yielded

good predictions of the R-curve behavior in these materials.<sup>[14]</sup> Third, as the bridging zones were measured from specimens precracked at stress-intensity ranges within 0.5 MPa√m of the threshold, it is conceivable that the measured values slightly overestimated the minimum bridging zone lengths.

#### 2. Crack-arrester orientation

By equating  $K_{o,max}$  to the measured  $K_{max,TH}$  values and using the experimentally measured fatigue bridging-zone lengths for the 50, 125, and 250 μm thick Nb laminates, corresponding predictions for the applied  $K_{max}$  values on the arrester fatigue curves were calculated for the highest constant  $\Delta K$  levels using Eq.[6] (Figure 10). The weight function for an SE(B) beam (Eq. [A2], Table A2) was used for 50 and 250 μm thick Nb laminates and for a C(T) specimen (Eq.[A2], Table A3) for 125 μm thick Nb material. The effective volume fractions were taken from Table I and the traction functions from Reference 14. Note that only the applied  $K_{max}$  values were predicted, and the corresponding experimental growth rates were assumed to apply to both the measured and the calculated  $K_{max}$  levels. The predictions for this orientation (Figure 10) slightly overestimate the experimentally observed  $K_{max}$  values at the highest applied  $\Delta K$  level for each laminate thickness. It is again believed that the limiting assumptions made on the bridging traction function are responsible for these discrepancies. However, based upon the previous modeling, the combination of the intrinsic effect of crack renucleation and extrinsic effect of crack bridging by intact Nb layers provides a rational description of the improved fatigue crack-growth resistance of the arrester laminates.

## IV. CONCLUSIONS

Based on an experimental and theoretical study of the fatigue-crack propagation behavior of laminated Nb-reinforced Nb<sub>3</sub>Al matrix composites, processed with Nb/Nb<sub>3</sub>Al layer thicknesses of, respectively, 50 μm/200 μm, 125 μm/500 μm, and 250 μm/1000 μm, with a constant volume fraction of (nominally) 20 vol pct Nb reinforcement, the following conclusions can be made.

1. High aspect-ratio ductile-phase reinforcements in the form of laminates are found to be effective at improving the crack-growth resistance of the intermetallic Nb<sub>3</sub>Al in both the crack-arrester and crack-divider orientations. Specifically, the fatigue crack-growth thresholds of all laminates were some 7 times higher than for unreinforced Nb<sub>3</sub>Al and more than twice that of a Nb particulate-reinforced Nb<sub>3</sub>Al (containing twice the volume fraction of Nb).
2. In both laminate orientations, superior fatigue-crack growth properties were found with the coarser laminate structures, primarily because the thicker Nb layers resulted in larger bridging zones in the crack wake.
3. For a given layer thickness, properties were better in the crack arrester than in the crack divider orientation. In the divider orientation, laminate properties were essentially bounded by the individual fatigue resistance of Nb and Nb<sub>3</sub>Al. In the arrester orientation, however, the composite displayed superior fatigue resistance to that of Nb and Nb<sub>3</sub>Al. This may be associated with trapping of the

entire crack front by the Nb reinforcing layers in the arrester orientation.

- The superior properties of the divider and arrester laminates are considered to result from intrinsic toughening due to trapping at, and crack renucleation across (arrester orientation only), the Nb layers and from extrinsic shielding from extensive crack bridging by intact Nb layers in the crack wake. In addition, non-coplanar cracking in the intermetallic, on either side of the reinforcing Nb layer, led to highly angled and tortuous crack paths in the reinforcing metal layer, thereby increasing the energy required to fail the bridging layer.
- Weight-function methods (using bridging traction functions derived under monotonic loading conditions) were moderately successful at modeling the effect of the crack bridging and, hence, in predicting the fatigue thresholds and/or crack-growth behavior of the laminates.

### ACKNOWLEDGMENTS

This work was funded by the Air Force Office of Scientific Research under the AASERT Program (Grant No. F49620-93-1-0441) as a supplement to Grant No. F49620-93-1-0107. The authors thank Dr. C.H. Ward for his support and Drs. B.J. Dalgleish and L.C. DeJonghe for their help with the composite processing.

### APPENDIX

#### Weight functions for compact-tension and single-edge-notched bend specimens

The weight function for the DC(T) specimen, as determined by Fett,<sup>[31]</sup> can be expressed as

$$h(a, x) = \sqrt{\frac{2}{\pi a}} \cdot \frac{1}{\sqrt{1 - \frac{x}{a}} \cdot \left(1 - \frac{a}{W}\right)^{3/2}} \quad [A1]$$

$$\left[ \left(1 - \frac{a}{W}\right)^{3/2} + \sum_{(\nu, \mu)} D_{\nu\mu} \cdot \left(1 - \frac{x}{a}\right)^{\mu+1} \cdot \left(\frac{a}{W}\right)^{\nu} \right]$$

where  $a$  is the crack length,  $W$  is the specimen width,  $x$  is the distance behind the crack tip measured from the load line, and the coefficients,  $D_{\nu\mu}$  (where  $\nu$  and  $\mu$  are simply indexes), for the sum are given in Table A1.

Similarly, the weight function for the SE(B) bending geometry (with a half outer span to width ratio greater than unity) is given by<sup>[25]</sup>

$$h(a, x) = \sqrt{\frac{2}{\pi a}} \cdot \frac{1}{\sqrt{1 - \frac{x}{a}}} \quad [A2]$$

$$\left[ 1 + \sum_{(\nu, \mu)} \frac{A_{\nu\mu} \cdot \left(\frac{a}{W}\right)^{\mu}}{\left(1 - \frac{a}{W}\right)^{3/2}} \cdot \left(1 - \frac{x}{a}\right)^{\nu+1} \right]$$

**Table A1. Coefficients of Fit Polynomial for DC(T) Weight Function**

$\nu$	$\mu = 0$	1	2	3	4
0	2.826	-5.865	0.8007	-0.2584	0.6856
1	-10.948	48.095	-3.839	1.280	-6.734
2	35.278	-143.789	6.684	-5.248	25.188
3	-41.438	196.012	-4.836	11.435	-40.140
4	15.191	-92.787	-0.7274	-7.328	22.047

**Table A2. Coefficients of Fit Polynomial for SE(B) Beam Weight Function**

$\nu$	$\mu = 0$	1	2	3	4
0	0.4980	2.4463	0.0700	1.3187	-3.067
1	0.5416	-5.0806	24.3447	-32.7208	18.1214
2	-0.19277	2.55863	-12.6415	19.7630	-10.986

**Table A3. Coefficients of Fit Polynomial for C(T) Weight Function**

$\nu$	$\mu = 0$	1	2	3	4
0	2.673	-8.604	20.621	-14.635	0.477
1	-3.557	24.9726	-53.398	50.707	-11.837
2	1.230	-8.411	16.957	-12.157	-0.940
3	-0.157	0.954	-1.284	-0.393	1.655

where  $x$  is measured from the specimen edge in this case, and the coefficients,  $A_{\nu\mu}$ , for the sum are given in Table A2.

The corresponding weight function for the C(T) geometry has the same form as Eq. [A2], except that  $x$  is measured from the load line.<sup>[25]</sup> There are also different coefficients,  $A_{\nu\mu}$ , for the sum; these are given in Table A3.

### REFERENCES

- P.A. Mataga: *Acta Metall.*, 1989, vol. 37 (12), pp. 3349-59.
- H.E. Dève, A.G. Evans, G.R. Odette, R. Mehrabian, M.L. Emilian, and R.J. Hecht: *Acta Metall. Mater.*, 1990, vol. 38 (8), pp. 1491-1502.
- M. Bannister and M.F. Ashby: *Acta Metall. Mater.*, 1991, vol. 39 (11), pp. 2575-82.
- T.C. Lu, A.G. Evans, R.J. Hecht, and R. Mehrabian: *Acta Metall. Mater.*, 1991, vol. 38 (8), pp. 1853-62.
- J. Kajuch, J. Short, and J.J. Lewandowski: *Acta Metall. Mater.*, 1995, vol. 43 (5), pp. 1955-67.
- S.M. Pickard and A.K. Ghosh: *Metall. Mater. Trans. A*, 1996, vol. 27A, pp. 909-21.
- K.T. Venkateswara Rao, G.R. Odette, and R.O. Ritchie: *Acta Metall. Mater.*, 1994, vol. 42 (3), pp. 893-911.
- K.T. Venkateswara Rao, G.R. Odette, and R.O. Ritchie: *Acta Metall. Mater.*, 1992, vol. 40 (2), pp. 353-361.
- G.R. Odette, B.L. Chao, J.W. Sheckhard, and G.E. Lucas: *Acta Metall. Mater.*, 1992, vol. 40 (9), pp. 2381-89.
- D.R. Bloyer, K.T. Venkateswara Rao, and R.O. Ritchie: *Mater. Sci. Eng. A*, 1996, vol. A216, pp. 80-90.
- D.R. Bloyer, K.T. Venkateswara Rao, and R.O. Ritchie: *Johannes Weertman Symp.*, R.J. Arsenault, D. Cole, T. Gross, G. Kostorz, P.K. Liaw, S. Parameswaran, and H. Sizek, eds., TMS, Warrendale, PA, 1996, pp. 261-66.
- D.R. Bloyer, K.T. Venkateswara Rao, and R.O. Ritchie: *Layered Materials for Structural Applications*, Materials Research Society Symposia Proceedings, J.J. Lewandowski, C.H. Ward, M.R. Jackson, and W.H. Hunt, Jr., eds., Materials Research Society, Pittsburgh, PA, 1996, vol. 434, pp. 243-48.
- D.R. Bloyer, K.T. Venkateswara Rao, and R.O. Ritchie: *Mater. Sci. Eng. A*, 1997, vol. A239-A240, pp. 393-98.

14. D.R. Bloyer, K.T. Venkateswara Rao, and R.O. Ritchie: *Metall. Mater. Trans. A*, 1998, vol. 29A, pp. 2483-96.
15. K. Badrinarayanan, A.L. McKelvey, K.T. Venkateswara Rao, and R.O. Ritchie: *Metall. Mater. Trans. A*, 1996, vol. 27A, pp. 3781-92.
16. L. Muruges, K.T. Venkateswara Rao, and R.O. Ritchie: *Scripta Metall. Mater.*, 1993, vol. 29, pp. 1107-12.
17. C.D. Bencher, A. Sakaida, K.T. Venkateswara Rao, and R.O. Ritchie: *Metall. Mater. Trans. A*, 1995, vol. 26A, pp. 2027-33.
18. P.C. Paris and F. Erdogan: *J. Bas. Eng., Trans. ASME*, 1963, vol. 85, pp. 528-34.
19. R.H. Dauskardt, M.R. James, J.R. Porter, and R.O. Ritchie: *J. Am. Ceram. Soc.*, 1992, vol. 75 (4), pp. 759-71.
20. J.P. Campbell, A.L. McKelvey, S. Lillibridge, K.T. Venkateswara Rao, and R.O. Ritchie: in *Deformation and Fracture of Ordered Intermetallic Materials III*, W.O. Soboyejo, T.S. Srivatsan, and H.L. Fraser, eds., TMS, Warrendale, PA, 1996, pp. 141-57.
21. R.O. Ritchie: *Int. Met. Rev.*, 1979, vol. 20 (5-6), pp. 205-30.
22. S. Suresh and R.O. Ritchie: in *Fatigue Crack Growth Threshold Concepts*, D.L. Davidson and S. Suresh, eds., TMS-AIME, Warrendale, PA, 1984, pp. 227-61.
23. C.J. Gilbert, R.H. Dauskardt, and R.O. Ritchie: *J. Am. Ceram. Soc.*, 1995, vol. 78 (9), pp. 2291-2300.
24. R.O. Ritchie: *Mater. Sci. Eng. A*, 1988, vol. A103, pp. 15-28.
25. T. Fett and D. Munz: "Stress Intensity Factors and Weight Functions for One-Dimensional Cracks," Institut für Materialforschung, Kernforschungszentrum Karlsruhe, Germany, 1994.
26. B.N. Cox and D.B. Marshall: *Acta Metall. Mater.*, 1991, vol. 39 (4), pp. 579-89.
27. B.N. Cox and C.S. Lo: *Acta Metall. Mater.*, 1992, vol. 40 (1), pp. 69-80.
28. F. Erdogan and P.F. Joseph: *J. Am. Ceram. Soc.*, 1989, vol. 72 (2), pp. 262-70.
29. R.M.L. Foote, Y.W. Mai, and B. Cotterell: *J. Mech. Phys. Solids*, 1986, vol. 34 (6), pp. 593-607.
30. A.C. Kaya and F. Erdogan: *Int. J. Fract.*, 1980, vol. 16 (2), pp. 171-90.
31. T. Fett: *Int. J. Fracture*, 1993, vol. 63, pp. R81-R85.